Preparation of a Novel Super Active Fischer-Tropsch Cobalt Catalyst Supported on Carbon Nanotubes

Tavasoli, Ahmad*[+]***; Irani, Mohammad; Nakhaeipour, Ali***
Research Institute of Petroleum Industry (RIPI), P.O. Box 18745-4163 Tehran, I.R. IRAN

Mortazavi, Yadollah; Khodadadi, Abas Ali
Department of Chemical Engineering, University of Tehran, P.O. Box 11365-4563 Tehran, I.R. IRAN

Ajay K. Dalai
Department of Chemical Engineering, University of Saskatchewan, Saskatoon, SK, S7N5C5, CANADA

ABSTRACT: *The potential of carbon nanotubes (CNT) supported cobalt catalysts for Fischer-Tropsch (FT) reaction is shown. Using the wet impregnation method cobalt on carbon nanotubes catalysts were prepared with cobalt loading varying from 15 to 45 wt. %. The catalysts are characterized by different methods including: BET physisorption, X-ray diffraction, hydrogen chemisorption, and temperature-programmed reduction. The activity and product selectivity of the catalysts were assessed and compared with alumina supported cobalt catalysts using a continuous-stirred tank reactor (CSTR). Using carbon nanotubes as cobalt catalyst support was found to decrease the reduction temperature of Co_3O_4 to CoO from 440 to 347 ^oC and that of CoO to Co^o from 640 to 574 ^oC. The strong metal-support interactions are reduced to a large extent and the reducibility of the catalysts improved by 67.7 %. CNT aided in well dispersion of metal clusters and average cobalt clusters size of the reduced cobalts is decreased from 5.3 to 4.9 nm. Results are presented showing that the hydrocarbon yield obtained by CNT supported cobalt catalyst is 74.6 % more than that obtained from cobalt on alumina supports. The maximum concentration of active surface Co^o sites and FTS activity for CNT supported catalysts are achieved 40 wt. % cobalt loading. CNT caused a slight decrease in the FTS product distribution to lower molecular weight hydrocarbons.*

KEY WORDS: *Fischer-Tropsch synthesis, Cobalt, Carbon nanotube, Reducibility, Reaction rate.*

INTRODUCTION

The Fischer-Tropsch synthesis (FTS) process has shown to be catalyzed by certain transition metals, with Co, Fe, and Ru presenting the highest activity [1-15]. Among them, cobalt catalysts are the preferred catalysts for FTS based on natural gas because of their high activity for FTS, high selectivity to linear hydrocarbons,

* *To whom correspondence should be addressed.*
+ E-mail: tavassolia@ripi.ir
1021-9986/09/1/37 11/$/3.10

Table 1: The composition of the catalysts.

Catalyst Name	A_1	C_1	C_2	C_3	C_4	C_5
Support	γ-Al_2O_3	CNT	CNT	CNT	CNT	CNT
Wt. % Cobalt	15	15	25	35	40	45

low activity for the water gas shift (WGS) reaction, more stable toward deactivation by water (a by-product of the FTS reaction), and low cost compared to Ru [1-8]. In order to achieve high surface active sites (Co^o), cobalt precursors are dispersed on porous carriers, with SiO_2, Al_2O_3, and to a lesser extent TiO_2 being the most frequently used [5-8].

A drawback of these support materials is their reactivity toward cobalt, which during preparation or catalysis results in the formation of mixed compounds that are reducible only at high reduction temperatures [5-8]. To avoid these problems, the use of carbon as a support has been explored [9-11]. Activated carbon has many advantages if utilized as FTS catalyst support (resistance to acidic or basic media, stable at high temperatures, etc.). Carbon nanotubes (CNT) possess similar properties and in most cases outperform activated carbon in this respect [5,11]. CNT have many unique structural properties and have attracted increasing attention as a novel support media for heterogeneous catalysis [5,11].

The present work was undertaken with the aim of exploiting the beneficial effects of carbon nanotubes support on performance on cobalt catalysts for FT synthesis. We varied the cobalt loadings from 15 to 45 wt. %. We assessed the physico-chemical characteristics and catalytic performance of the catalysts and compared the results with an alumina supported cobalt catalyst.

EXPERIMENTAL

Catalyst preparation

Conndea Vista Catalox B γ–alumina and multiwall purified (> 95 %) RIPI-CNT were used as support materials for the preparation of cobalt FTS catalysts. The CNT support was treated with 30 wt. % HNO_3 at 100 ^oC over night. One γ–alumina supported catalyst (A_1) was prepared with cobalt loading of 15 wt. % and five carbon nanotube supported catalysts (C_1-C_5) were prepared with loadings of 15, 25, 35, 40 and 45 wt. %. The catalysts were prepared using an aqueous solution of cobalt nitrate ($Co(NO_3)_2.6H_2O$ 99.0 %, Merck).

The sequential impregnation method was used to add cobalt to the supports [5, 6]. After each step, catalysts were dried at 120 ^oC. The alumina supported catalyst was calcined at 450 ^oC for 3 h [5, 6] and CNT supported catalysts were calcined at 350 ^oC for 3 h (determined by TGA analysis, see next section) with a heating rate of 1 ^oC /min. The cobalt loadings were verified by an inductively coupled plasma (ICP) system. The catalysts nomenclature and compositions are listed in table 1.

Thermogravimetric analysis (TGA)

Perkin Elmer Thermogravimetric differential thermal analyzer was used to measure weight changes of the C_1 sample when heated under a flow of argon (flow rate of 40 mL/min) at a constant heating rate of 10 °C/min.

Transmission Electron Microscopy (TEM)

The treated CNT and C_1 catalyst were characterized by Transmission Electron Microscopy (TEM). Sample specimens for TEM studies were prepared by ultrasonic dispersion of the CNTs and catalysts in ethanol. The suspensions were dropped onto a carbon-coated copper grid. TEM investigations were carried out using a Hitachi H-7500 (120 kV).

Scanning electron microscopy (SEM)

The treated CNT and C_1 catalyst were characterized by scanning electron microscopy (SEM). SEM analysis was carried out using a Hitachi S-4700 at 3 kV. Sample specimens for SEM were prepared by ultrasonic dispersion of samples in methanol. The suspensions were dropped onto a silica support.

BET surface area measurements/ BJH pore size distributions

The surface area, pore volume, and average pore radius of the two supports and A_1 and C_1 catalysts were measured by an ASAP-2010 system from Micromeritics. The samples were degassed at 200 ^oC for 4 h under 50 mTorr vacuum and their BET area, pore volume, and average pore radius were determined.

X-ray diffraction

XRD measurements of the calcined A_1 and C_1 catalysts were conducted with a Philips PW1840 X-ray diffractometer with monochromatized Cu/K_α radiation. Using the Scherrer equation, the average size of the Co_3O_4 crystallites in the calcined catalysts was estimated from the line broadening of a Co_3O_4 at 2θ of 36.8°.

Temperature programmed reduction

Temperature programmed reduction (TPR) spectra of the calcined A_1 and C_1 catalysts were recorded using a Micromeritics TPD-TPR 290 system, equipped with a thermal conductivity detector. The catalyst samples were first purged in a flow of argon at 400 °C, to remove traces of water, and then cooled to 40 °C. The TPR of 50 mg of each sample was performed using 5.1 % hydrogen in argon gas mixture with a flow rate of 40 cm^3/min. The samples were heated from 40 to 900 °C with a heating rate of 10 °C /min.

Hydrogen chemisorption and reoxidation

The amount of chemisorbed hydrogen of the all catalysts was measured using the Micromeritics TPD-TPR 290 system. 0.25 g of the calcined catalyst was reduced under hydrogen flow at 400 °C for 12 h and then cooled to 100 °C under hydrogen flow. Then the flow of hydrogen was switched to argon at the same temperature, which lasted about 30 minutes in order to remove the weakly adsorbed hydrogen. Afterwards, the temperature programmed desorption (TPD) of the samples was obtained by increasing the temperature of the samples, with a ramp rate of 10 °C /min, to 400 °C under the argon flow. The TPD spectrum was used to determine the cobalt dispersion and its surface average crystallite size. After the TPD of hydrogen, the sample was reoxidized at 400 °C by pulses of 10 % oxygen in helium to determine the extent of reduction. It is assumed that Co^o is oxidized to Co_3O_4. The calculations are summarized below. The calculated dispersion and diameter are corrected by the percentage reduction [5,6].

$$\%\text{Dispersion}=\frac{\text{number of } Co^{\circ} \text{ atoms on surface}}{\text{number of Co atoms in sample}}\times 100 \quad (1)$$

$$\text{Fraction reduced}=\frac{O_2 \text{ uptake}\times 2/3\times \text{atomic weight}}{\text{Percentage metal}} \quad (2)$$

$$\text{Diameter}=\frac{6000}{\text{density}\times\text{maximum area}\times\text{dispersion}} \quad (3)$$

Reaction Testing

The catalysts were evaluated in terms of their Fischer-Tropsch synthesis (FTS) activity (g HC produced/ g cat./ h) and selectivity (the percentage of the converted CO that appears as a hydrocarbon product) in a continuous-stirred tank reactor (CSTR). Prior to the activity tests, the catalyst activation was conducted according to the following procedure. The catalyst (50 g) was placed in the CSTR and pure hydrogen was introduced at a flow rate of 60 NL/h. The reactor temperature was increased from room temperature to 400 °C at a rate of 1 °C/min, maintained at this activation condition for 24 h and the catalyst was reduced in-situ. After the activation period, the reactor temperature was decreased to 120 °C. Pure melted C_{28} paraffin wax was used as start-up media. C_{28} paraffin wax was degassed at degasser vessel with nitrogen at 120 °C for 1 h and transferred to the CSTR to mix with catalyst. Then the reactor temperature increased to 180 °C under flowing hydrogen. The FTS reactor system is shown in Fig. 1.

Separate Brooks 5850 mass flow controllers were used to add H_2 and CO at the desired rate to a mixing vessel that was preceded by a lead oxide-alumina containing vessel to remove carbonyls before entering to the reactor. The mixed gases entered through a dip tube to the bottom of the CSTR below the stirrer. The CSTR was operated at 750 rpm. The temperature of the reactor was controlled via a PID temperature controller. Synthesis gas with a flow rate of 90 NL/h (H_2/CO ratio of 2) was introduced and the reactor pressure was increased to 25 bars. The reactor temperature was then increased to 220 °C at a rate of 1 °C/min. products were continuously removed from the vapor and passed through two traps, one maintained at 100 °C (Hot Trap) and the other at 0 °C (Cold Trap). The uncondensed vapor stream was reduced to atmospheric pressure through a pressure letdown valve. The flow was measured with a bubble-meter every 1 hour and composition quantified using an on-line Varian 3800 gas chromatograph. The accumulated reactor liquid wax products were removed every 12 h by passing through a 2 μm sintered metal filter located below the liquid level in the CSTR. The contents hot and cold traps removed every 12 h, the hydrocarbon and water fractions separated, and then analyzed by GC.

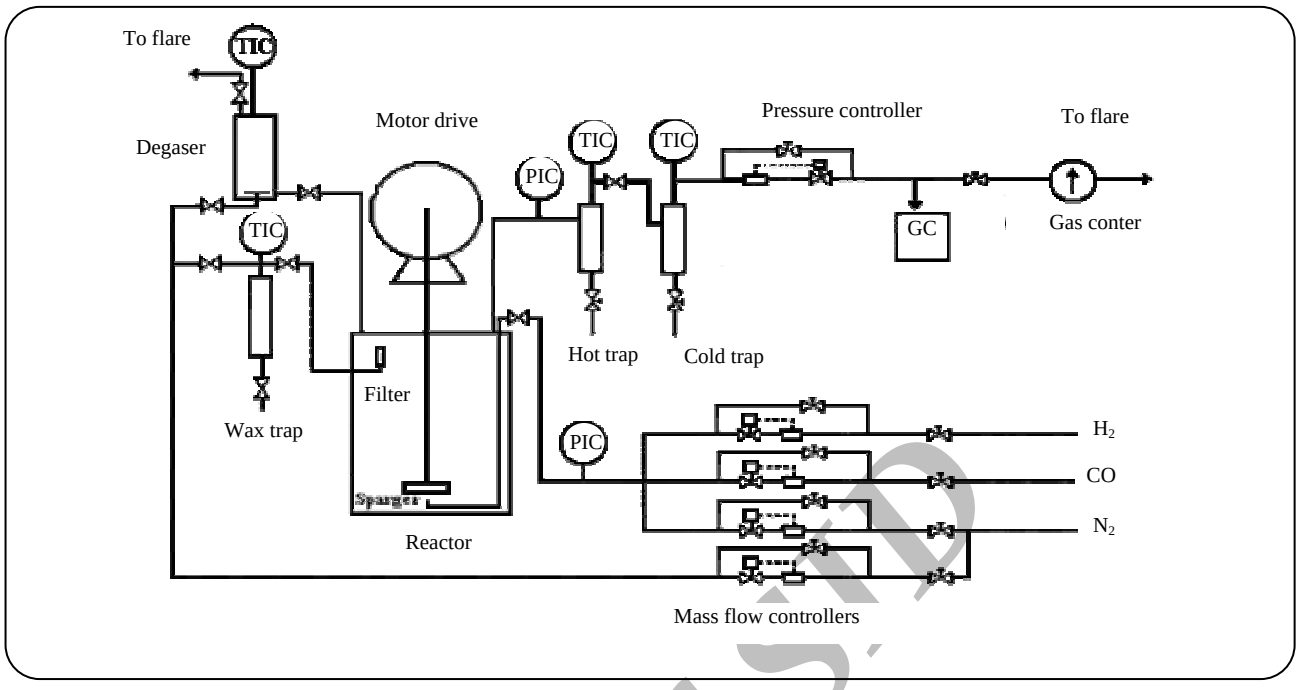

Fig. 1: Experimental setup.

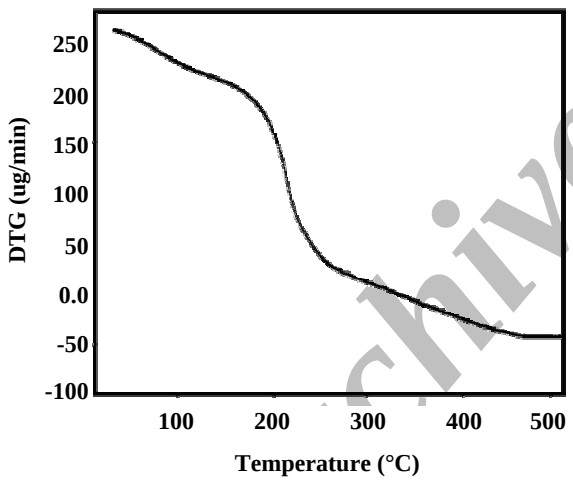

Fig. 2: Thermogravimetric analysis of C_1.

RESULTS AND DISCUSSION

The TGA technique was used to investigate the presence of any decomposable materials in the uncalcined C_1 catalyst. Fig. 2 shows the results of thermogravimetric analysis for C_1 catalyst. Results show that the rapid weight loss started below 200 °C and continued up to a temperature of 350 °C. Calcination of the CNT supported catalysts at 350 °C for 3 h was expected to remove all the displaceable water and counter ions present in the catalyst.

A sample of the purified CNT material was analyzed by TEM. The purified product is comprised of an interwoven matrix of tubes (Fig. 3) that was shown to be comprised of multi-walled carbon nanotubes (MWCNTs). The TEM images of C_1 catalyst revealed that the catalyst particles are well dispersed inside the tubes and also on the perimeter of the tube walls (Fig. 4). The particles inside the tubes are fairly uniform and the most abundant ones are 3-7 nm in size in accordance with the average inner diameter of the CNTs, whereas those on the outer surface have grown to about 8-12 nm (Fig. 4).

Obviously, the CNT channels have restricted the growth of the particles inside the tubes. Fig. 5 shows the scanning electron microscopy (SEM) picture of the CNTs. In addition to the catalyst particles visible in Fig. 4, the representative SEM image of C_1 catalyst shown in Fig. 6 reveals the small particles on or in the CNT walls. A bar graph depicting the size distribution of the particles which is taken using 10 TEM pictures is shown in Fig. 7. The average size of these small particles is 5 nm.

Results of surface area measurements are shown in table 2. The BET surface of the A_1 and C_1 catalysts are lower than that of the supports which indicates pore blockage due to cobalt loading.

Table 2: BET surface area and porosity data.

Support/Catalyst	BET (m^2/g)	Pore Volume (Single point) (cm^3/g)	Average Pore Radius (nm)
γ-Al_2O_3	270	0.639	4.72
CNT	497	1.034	4.16
A_1	214	0.439	4.26
C_1	372	0.765	4.38

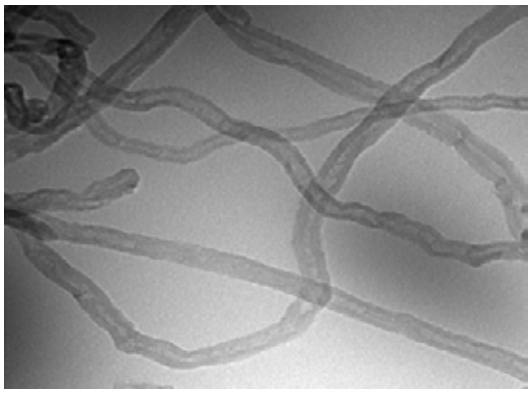

Fig. 3: TEM image of purified CNT.

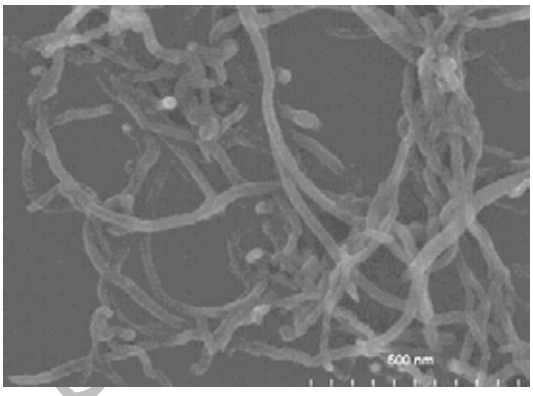

Fig. 5: SEM image of purified CNT.

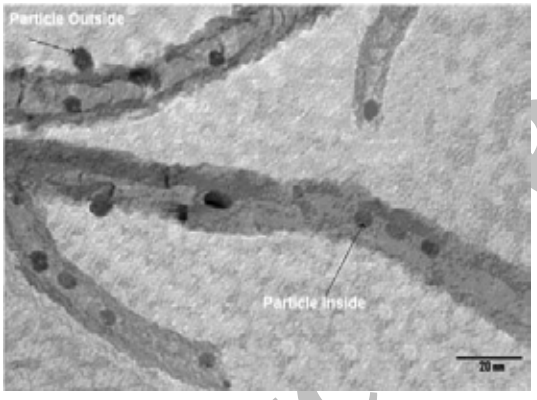

Fig. 4: TEM image of C_1 catalyst showing cobalt particles inside and outside of the tubes.

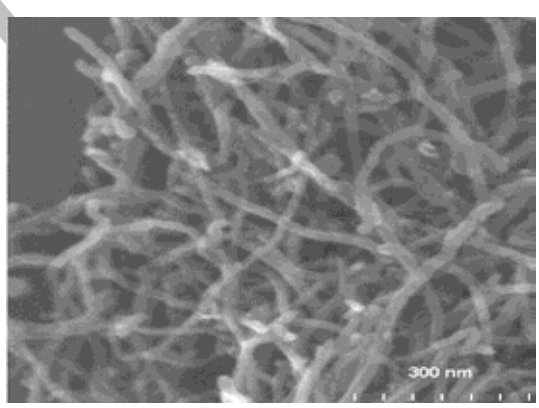

Fig. 6: SEM image of C_1 catalyst.

XRD patterns of the two supports and calcined A_1 and C_1 catalysts are shown in Fig. 8. In the XRD of γ-alumina support peaks at 46.1 and 66.5° correspond to Al_2O_3. Also the peaks at 46.1 and 66.5° in the XRD spectrum of A_1 catalyst correspond to γ-alumina, while the other peaks, except the 49° peak, which is attributed to the cobalt aluminate [5,6,12], relate to the different crystal planes of Co_3O_4. In the XRD spectrum of CNT support and C_1 catalyst, peaks at 25 and 43° correspond to carbon nanotube. While the other peaks in the spectrum of C_1 catalyst are related to the different crystal planes of Co_3O_4. In contrast to the 49° peak in the spectrum of A_1 catalyst, which is attributed to the cobalt aluminate, in the XRD spectrum of C_1 catalyst no peak was observed indicating formation of cobalt support compounds. The peak of 36.8° is the most intense peak of Co_3O_4 in XRD spectrum of A_1 and C_1 catalysts. Table 3 shows the average Co_3O_4 particle size of the catalysts calculated from XRD spectrum and Scherrer equation at 36.8° [5]. This table represents that the average Co_3O_4 crystallitesize in C_1 catalyst is smaller than A_1 catalyst. Higher surface area of CNT support in C_1 catalyst will

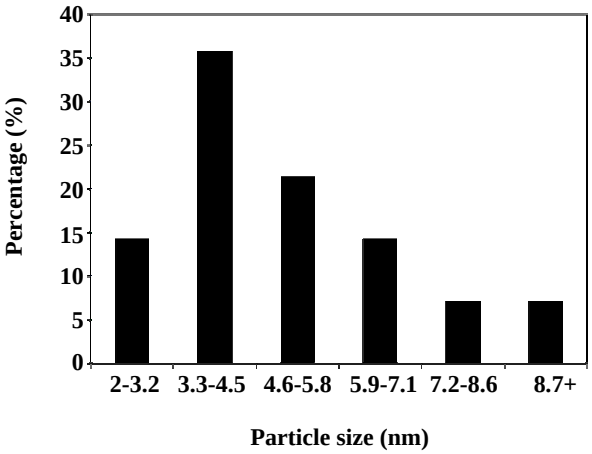

Fig. 7: A bar graph depicting the size distribution of the particles of C_1 catalyst.

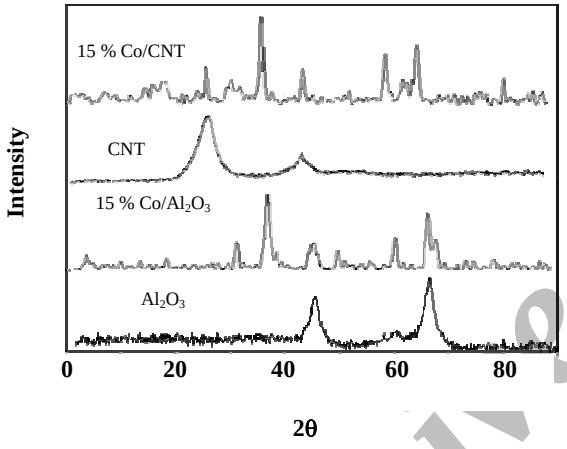

Fig. 8: XRD patterns of γ-alumina, CNT, calcined A_1 catalyst and calcined C_1 catalyst.

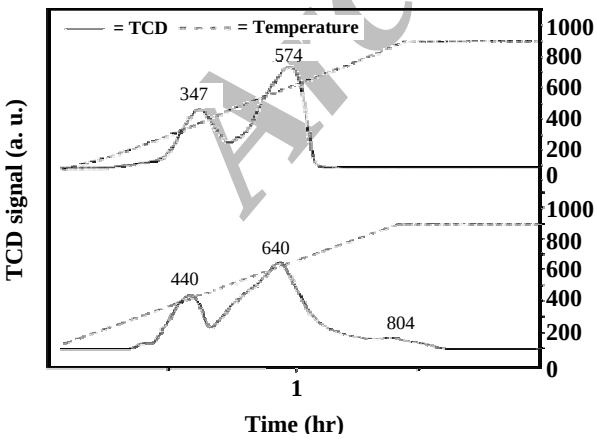

Fig. 9: TPR patterns of the calcined A_1 and C_1 catalysts from 40-1000 °C.

lead to better distribution of particles, which in turn leads to lower cobalt cluster sizes.

Temperature programmed reduction (TPR) is a powerful tool to study the reduction behavior of oxidize phases; in some cases it is also possible from the reduction profiles of supported oxides to obtain useful information about the degree of interaction of the active metal with the support [6,12]. The TPR spectra of the calcined A_1 and C_1 catalysts are shown in Fig. 9. In this Figure, in the TPR profile of A_1 catalyst the first peak is typically assigned to the reduction of Co_3O_4 to CoO, although a fraction of the peak likely comprises the reduction of the larger, bulk-like CoO species to Co^o. The second peak, with a broad shoulder is mainly assigned to the second step reduction, which is mainly reduction of CoO to Co^o. This peak also includes the reduction of cobalt species that interact with the support, which extends the TPR spectra to higher temperatures.

As shown in this Figure, interaction between the cobalt and alumina support shifts the reduction of some cobalt species to temperatures about 750 °C. Also a reduction feature for A_1 catalyst observed in the temperature range of 700-950 °C, with a maximum centered at about 804 °C. Such a high reduction temperature might be assigned to the reduction of cobalt aluminates the lower temperatures. It results in a decrease in the temperature of the first TPR peak from 440 to 347 °C and the temperature of the second TPR peak from 640 to 574 °C, suggesting an easier reduction process (Fig. 9 and table 3). Fig. 9 also indicates that using CNT as cobalt catalyst support eliminates the second TPR peak tailing, which reveals that in Co/CNT catalyst the degree of interaction between active metal and support is zero. This indicates that by using CNT as cobalt catalyst support, the amount of the species reduced at high temperatures (550-650 °C) decreases. Lack of interaction between cobalt and the CNT support is the main reason of decreasing the reduction temperatures. This will make more cobalt atoms to be available for FTS reaction in CNT supported cobalt catalysts in comparison with alumina supported cobalt catalysts. Table 3 also shows the amount of hydrogen consumed and the percentagespecies formed by reaction of highly dispersed CoO with the alumina. In fact, cobalt aluminates were shown to reduce at temperatures well above 800 °C,

Table 3: XRD and TPR data.

Catalyst	XRD d_{Co3O4} (nm)	1st TRR peak (°C)	2nd TRR peak (°C)	3rd TRR peak (°C)	H_2 Consumed (mole)	% Reduction
A_1	16.4	440	640	804	0.000157	92.6
C_1	13.2	347	574	-	0.000168	99.1

Table 4: H_2 temperatures programmed desorption and pulse reoxidation of catalysts.

Catalyst	μ mole H_2 desorbed /g cat.	μ mole O_2 Consumed /g cat.	% Red.	% Dispersion (Tot. Co)	% Dispersion (Red. Co)	d_p (nm) (Tot. Co)	d_p (nm) (Red. Co)
A_1	76.52	601.29	32.00	6.02	18.81	16.61	5.32
C_1	139.81	1008.48	53.67	11.01	20.52	9.17	4.92
C_2	173.31	2195.96	70.12	8.18	11.67	12.46	8.72
C_3	150.38	3783.74	86.30	5.07	5.9	19.72	17.00
C_4	135.59	4494.53	90.80	4.10	4.51	23.41	20.76
C_5	121.10	5012.29	90.01	3.18	3.53	29.25	26.33

while bulk Co_3O_4 became completely reduced at temperatures below 500 °C [6,12]. All these features suggest part of the cobalt in the alumina supported cobalt catalysts strongly interacts with the support, as also evidenced from XRD patterns. Fig. 9 also shows the TPR of the CNT supported cobalt catalyst. This Figure shows that, using CNT, as cobalt catalyst support will shift both TPR peaks significantly to reduction for A_1 and C_1 catalysts during TPR tests. Assuming that the major species of the calcined Co catalyst is Co_3O_4, the amount of H_2 that can be consumed at 100 % reducibility of 50 mg of 15 wt. % cobalt catalysts is 0.0001695 moles [5]. As shown in table 3, CNT also enhances the reducibility of both Co_3O_4 and other Co oxide species, as indicated by the amount of hydrogen consumption and the reducibility. The enhancement of reducibility can be attributed to the lack of interaction between cobalt and the CNT support.

The results of hydrogen temperature programmed desorption (TPD) and oxygen titrations of the calcined catalysts are given in table 4. For each sample, uncorrected dispersion and particle size were calculated based on the total amount of cobalt in the catalyst samples. The percentage of reduction was measured from the oxygen titration after TPD, assuming Co^o is reoxidized to Co_3O_4. The calculated dispersion and average particle size are corrected by the percentage reduction.

Comparing the results of TPD and oxygen titrations of the calcined A_1 and C_1 catalysts on table 4, it is clear that, the hydrogen uptake increases up to 2 fold by using CNT as cobalt catalyst support. In agreement with the results of TPR, results in this Table indicate that a remarkable improvement in the percentage reduction is obtained by switching to CNT support with the same loading. While the dispersion of the cobalt crystallites calculated based on the total amount of cobalt and the amount of reduced cobalt increases significantly, the average cobalt particle size decreases which is due to higher surface area of CNT, lower degree of aglomerization of the cobalt crystallites and lower interaction of cobalt with support in CNT supported catalyst. Larger dispersion and lower cobalt cluster size will increase greatly the number of sites available for FT reaction in CNT supported catalysts with the same loading.

This table shows that for CNT supported catalysts the hydrogen uptake increases with increasing the amount of cobalt added up to 25wt. % then decreases. The percentage reduction increases with the increasing of the amount of cobalt up to 40wt % then starts to decrease. Also it shows that by increasing the cobalt loading the dispersion of the cobalt crystallites decreases significantly. This table shows that increasing the amount of cobalt causes a remarkable increase in cobalt particle size, which is due to the aglomerization of the cobalt crystallites with increasing the cobalt loading. The improvements in the percentage reduction with increasing the cobalt loading for CNT supported catalysts can be attributed to the easier reduction of larger cobalt clusters [5,12].

$$R_{WGS} = R_{FCO2} = \text{g } CO_2 \text{ produced / g cat. / h} \quad (4)$$

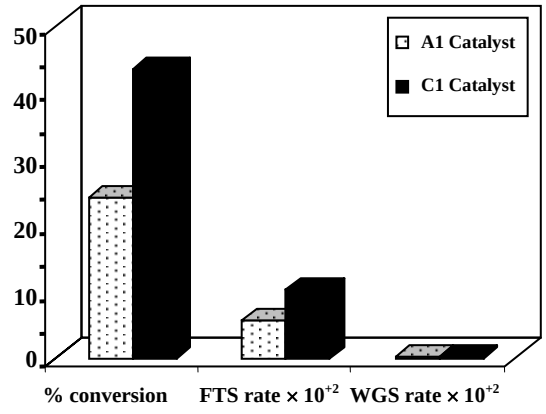

*Fig. 10: FTS rate * 10^2(g HC/g cat./hr), % CO Conversion, WGS rate* 10^2 (g CO_2/g cat./hr) of the A_1 and C_1 catalysts ($T = 220\ ^oC$, P = 25 bar and $H_2/CO = 2$).*

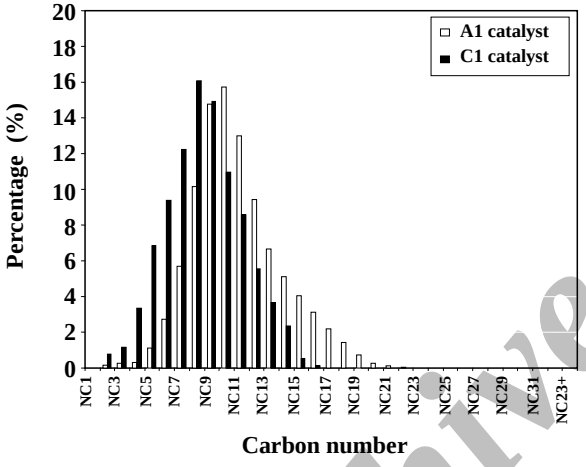

Fig. 11: Cold trap product distributions for A_1 and C_1 catalysts ($T = 220\ ^oC$, P = 25 bar and $H_2/CO = 2$).

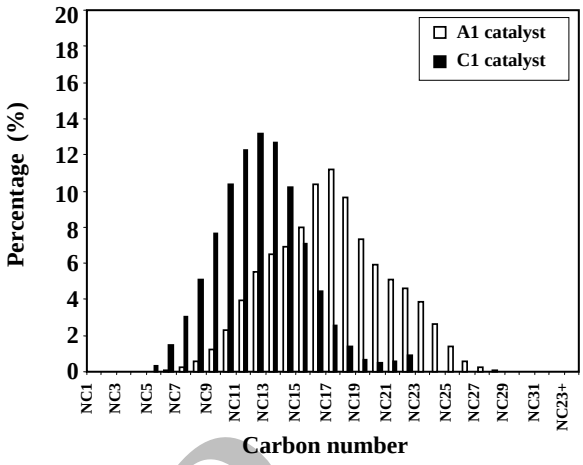

Fig. 12: Hot trap product distributions for A_1 and C_1 catalysts ($T = 220\ ^oC$, P = 25 bar and $H_2/CO = 2$).

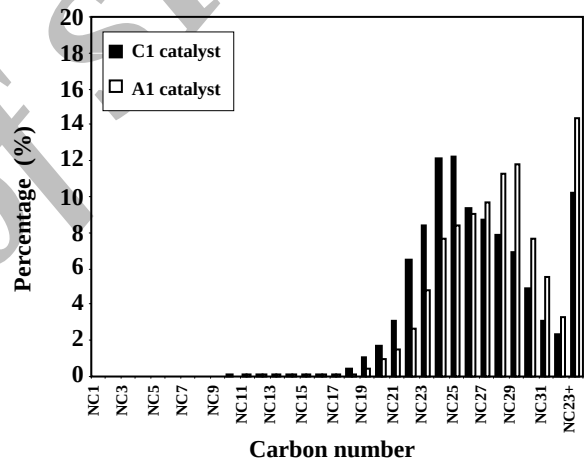

Fig. 13: Wax trap product distributions for A_1 and C_1 catalysts ($T = 220\ ^oC$, P = 25 bar and $H_2/CO = 2$).

Fig. 10 reveals that using CNT as cobalt catalyst support dramatically enhances the CO conversion, FT synthesis and water gas shift reaction rates. However, the effect on the water gas shift reaction rate is less pronounced. CO conversion and the FTS rate show an increase of about 75 % in accordance with hydrogen uptake, percentage reduction and percentage dispersion (table 4). Also WGS rate shows about 58 % increase. Fig. 10 and table 4 reveal that the FTS rate and CO conversion are strongly dependent and proportional to the number of surface reduced active cobalt sites. This Figure shows that the water gas shift reaction rate increases when CNT is used as cobalt catalyst support. The increase of the WGS reaction rate or CO_2 formation rate can be attributed to the increase in water partial pressure, due an increase in FTS reaction rate in C_1 catalyst [5].

Figs. 11, 12 and 13 show the effects of support on the selectivity of Fischer-Tropsch synthesis products. Comparing the product distributions of the cold trap, hot trap and wax trap for A_1 and C_1 catalysts, clearly demonstrate that, unlike to the significant improvement in the CO conversion and FTS rate, product distribution shows a distinct shift to lower molecular weight hydrocarbons in CNT supported cobalt catalyst. Calculations show that the methane selectivities for A_1 and C_1 catalysts are 8.95 % and 12.10 % respectively. Also the selectivity to liquid C_{5+} products for A_1 and C_1 catalysts are 87.09 % and 81.26 % respectively.

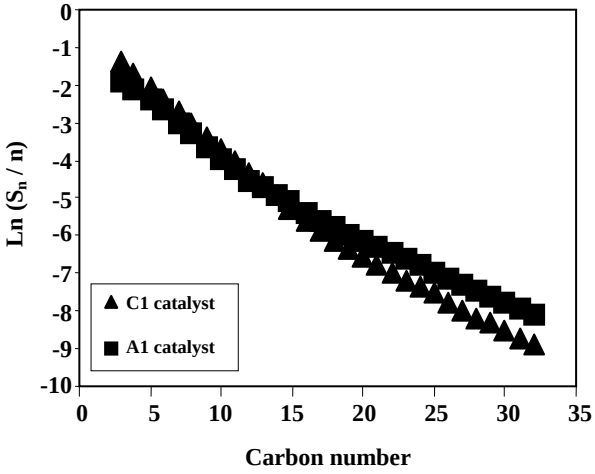

Fig. 14: ASF distribution of FTS products on A_1 and C_1 catalysts (T = 220 °C, P = 25 bar and H_2/CO = 2).

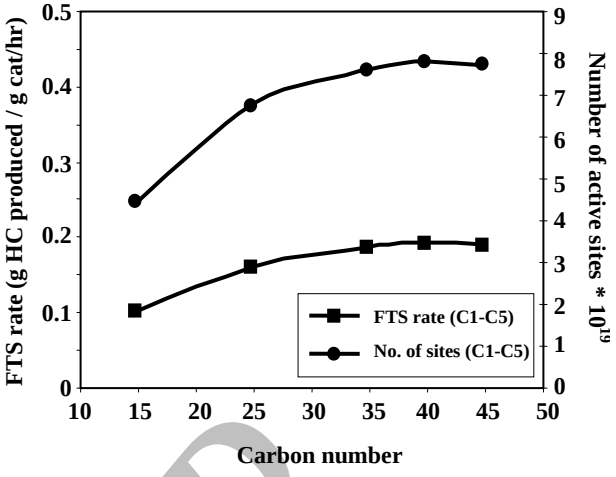

Fig. 15: Variation of FTS rate (g HC produced/ g cat/hr) and number of active sites with cobalt loading for CNT supported catalysts (T = 220 °C, P = 25 bar and H_2/CO = 2).

C_{5+} selectivity is decreased by 5.83 % and CH_4 selectivity is increased by 3.06 % for CNT supported catalyst. It is believed that in FTS the larger cobalt particles are more selective to higher molecular weight hydrocarbons and the smaller particles are selective for methane and light gases [5,12]. It seems that that in A_1 catalyst, which has larger cobalt c lusters (table 4), the steric hindrance for dissociative adsorption of CO and -CH_2- monomer and addition of this monomer to the growing chain is less. On the other hand, chain propagation and growth probability at the surface of the large clusters of A_1 catalyst is more than that of the smaller clusters of C_1 catalyst.

Anderson-Schultz- Floury (A-S-F) distribution of FTS products on A_1 and C_1 catalysts is presented in Fig. 14. Product distribution shows a distinct shift to higher molecular weight hydrocarbons in A_1 catalyst. The trend lines were plotted for C_3^+ products to determine the chain growth probability, α. The chain growth probability was 0.89 and 0.85 for A_1 and C_1 catalysts respectively, which again stresses the higher molecular weight hydrocarbons production in A_1 catalyst.

Fig. 15 presents the results of FT synthesis rate and number of active sites for different CNT supported cobalt catalysts. The number of active cobalt sites was defined as [5]:

$$\text{No.of Active Sites} = \frac{\text{wt. of Co} \times \text{Fraction Red.} \times \text{Dispersion} \times N_A}{MW} \quad (5)$$

Where NA is Avogadro's number and MW is molecular weight of cobalt. Fig. 15 shows that for CNT supported cobalt catalysts the FTS rate and the numbers of active cobalt sites show a remarkable increase with increasing the amount of cobalt loading up to 40 wt. % then slightly decrease. This Figure also shows that the Fischer-Tropsch activity of the CNT supported catalysts is strongly proportional to the number of active cobalt sites. For CNT supported catalysts the maximum activity and the maximum concentration of surface Co^o sites were obtained at 40 wt. % cobalt loading. In our previous work we have studied the cobalt loading effects on the structure and activity for FTS and WGS reactions of alumina supported cobalt (Co/Al_2O_3) catalysts [12]. We varied the cobalt loading from 8 to 40 wt. %. We have shown that in the case of alumina supported cobalt catalysts by increasing the amount of cobalt loading, FTS rate and number of active cobalt sites increases, passes through a maximum at cobalt loading of 34 wt. % and then starts to decrease [12]. So we can conclude that for alumina supported catalysts; the maximum FTS activity can be achieved at the 34 wt. % while for CNT supported catalysts the maximum FTS activity can be achieved at the 40 wt. % of cobalt loading.

Comparing the results on Fig. 15 and our pervious data [12] show that, higher surface area and higher pore volume of the CNT were allowed to load more cobalt and have more surface Co^o sites on the CNT supported catalysts than the alumina supported catalysts.

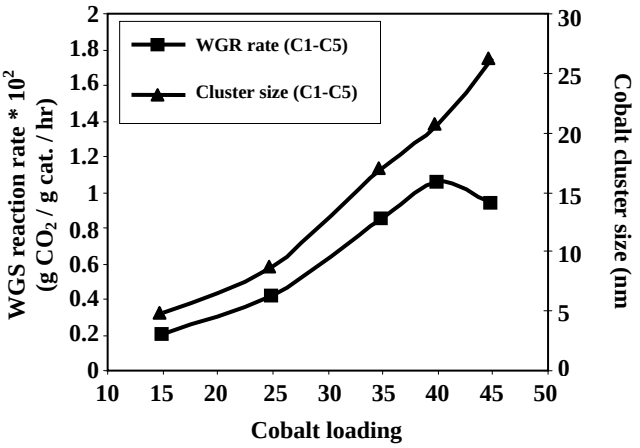

Fig. 16: Variation of WGS reaction rate 10^2 (g CO_2/g cat./hr) and cobalt cluster size (nm) with cobalt loading for CNT supported catalysts (T = 220 °C, P = 25 bar and H_2/CO = 2).*

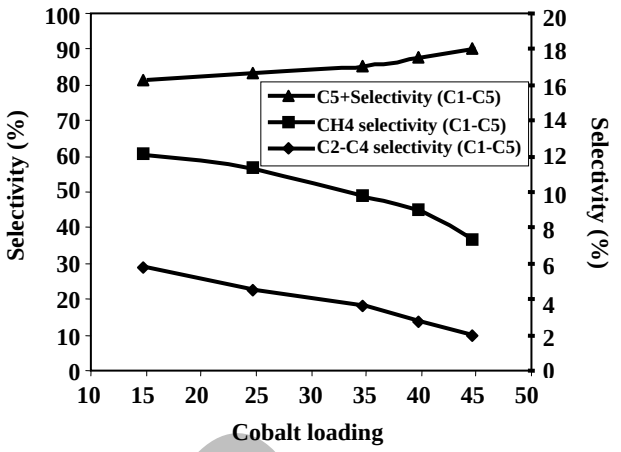

Fig. 17: Variation of CH_4, C_2-C_4 and C_{5+} selectivity of FTS with cobalt loading for CNT supported catalysts (T = 220 °C, P = 25 bar and H_2/CO = 2).

Consequently, not only CNT supported catalysts are more active than the alumina supported catalysts with the same loading, but also the amount of maximum cobalt loading on the CNT is higher than the alumina supports. FT synthesis with the CNT supported catalysts which have higher volumetric productivity will decrease reactor volume. In addition to the above-mentioned characteristics, carbon nano tubes have many unique structural properties, higher resistance to acidic medias, higher resistance to basic medias and have higher stability at high temperatures, etc.

Therefore, carbon nano tubes can outperform oxide supports like Al_2O_3, SiO_2 and TiO_2 if utilized as FTS catalyst support. Since FT reaction is not a fast reaction, industrial scale FT reactors have huge dimensions (i.e. for a reactor with 15000 bbl/day production rate: Diameter = 10 m, Height = 40 m). Therefore, using this inventive CNT supported cobalt catalyst can decrease the industrial scale reactors volume by about 50 % [5] and improve process economics significantly. On the other hand in order to increase the reducibility and activity of the conventional metal oxide supported cobalt catalysts, ruthenium and rhenium are used as cobalt catalyst promoters. Indeed, these promoters can increase the reducibility and activity of the conventional metal oxide supported cobalt catalysts, the application of ruthenium and rhenium as cobalt catalyst promoters in FTS is restricted due to their high price. Excellent reducibility and high activity of CNT supported cobalt catalysts makes it a suitable candidate for industrial FT processes and eliminate the need for such costly promoters. However, it is to note that despite the advantages mentioned for CNT's, they have some disadvantages. A low metal-support interaction could result in higher sintering rate and higher deactivation rate which should be studied. Also their mechanical characteristics should be improved by addition of some binders.

The effect of the cobalt loading on cobalt cluster size and water gas shift reaction rate for different CNT supported cobalt catalysts are shown in Fig. 16. This Figure shows that, the cobalt cluster size increases by increasing the cobalt loading while the water gas shift reaction rate increases by increasing the cobalt loading up to 40 wt. % and then starts to decrease. This may be attributed to the tendency of larger cobalt particles for H_2O adsorption, which presumably participate in the water-gas shift reaction, and leads to the production of CO_2. Also, the increase of the CO_2 formation rate can be attributed to the increase in water partial pressure, due an increase in FTS reaction rate [5,12].

Fig. 17 shows the effect of cobalt loading on the hydrocarbon selectivity of Fischer-Tropsch synthesis to CH_4 C_2-C_4, and C_{5+} products for different CNT supported cobalt catalysts. It clearly shows that, the methane selectivity reduces and that of C_{5+} increases by increasing the cobalt loading. Moving upward from the 15 to 45 wt. % cobalt loaded catalyst result in 11 % improvement in the C_{5+} selectivity of the CNT supported cobalt catalysts. At the same time the CH_4 selectivity of the CNT supported cobalt catalysts decreased by 29.9 %.

Also the C_2-C_4 light gaseous hydrocarbons selectivity is decreased by about 60 %. So, in the case of selectivity 45 wt. % Co/CNT is the best catalyst. The results of this Figure and table 4 clearly demonstrate that the larger cobalt particles are more selective to higher molecular weight hydrocarbons and the smaller particles are selective for methane. [5,12,13].

CONCLUSIONS

TPR and H_2 chemisorption with pulse reoxidation screenings indicated that by using carbon nanotubes as cobalt catalyst support the interaction between cobalt surface species decreased greatly. The reduction temperature of cobalt oxide species shifted to lower temperatures and the reducibility of the catalyst improved significantly. CNT aided in well dispersion of metal clusters and average cobalt clusters size decreased. From a catalytic activity standpoint, the Fischer-Tropsch synthesis rate and percentage CO conversion obtained by carbon nanotubes as cobalt catalysts were amazingly much larger than that obtained from cobalt on alumina support. The maximum concentration of active surface Co^o sites and FTS activity for CNT supported catalysts are achieved at 40 wt. % cobalt loading. CNT caused a slight decrease in the FTS product distribution to lower molecular weight hydrocarbons.

Nomenclatures

P	Pressure (bar)
T	Temperature (^{o}C)
R	Rate (g/g cat. /min)
S	Selectivity (%)

Abbreviations

FTS	Fischer-Tropsch Synthesis
WGS	Water-gas shift
RIPI	Research Institute of Petroleum Industry
CNT	Carbon nano tube
XRD	X-ray diffraction
TPR	Temperature programmed reduction
GC	Gas chromatograph
TPD	Temperature programmed desorption
ICP	Inductively coupled plasma

Subscripts

n	Carbon number
f	Formation
p	Particle

Received : 28th April 2007 ; Accepted : 26th August 2008

REFERENCES

[1] Oukaci, R., Singleton, A. H., Goodwin, J. G., Comparison of Patented Co FT Catalysts Using Fixed-Bed and Slurry Bubble Column Reactors, *Applied catalysis A: General*, **186**, 129 (1999).

[2] Iglesia, E., Design, Synthesis and Use of Cobalt-Based Fischer-Tropsch Synthesis Catalysts, *Applied Catalysis A: General*, **161**, 59 (1997).

[3] Bechara, R., Balloy, D., Vanhove, D., Catalytic Properties of Co/Al_2O_3 System for Hydrocarbon Synthesis, *Applied Catalysis A: General*, **207**, 343 (2001).

[4] Steen, E. V., Prinsloo, F. F., Comparison of Preparation Methods for Carbon Nanotubes Supported Iron FT Catalysts, *Catalysis Today*, **71**, 327 (2002).

[5] Tavasoli, A., Catalyst Composition and its Distribution Effects on the Enhancement of Activity, Selectivity and Suppression of Deactivation Rate of FTS Cobalt Catalysts, Ph.D. Thesis, University of Tehran (2005).

[6] Tavasoli, A., Mortazavi, Y., Khodadadi, A., Sadagiani, K., Effects of Different Loadings of Ru and Re on Physico-Chemical Properties and Performance of 15 % Co/Al_2O_3 FTS Catalysts, *Iranian Journal of Chemistry and Chemical Engineering*, **35**, 9 (2005).

[7] Van Berge, P.J., van de loosdrecht, J., Barradas, S., can der karaan, A. M., Oxidation of Cobalt Based Fischer-Tropsch Catalysts as a Deactivation Mechanism, *Catalysis Today*, **58,** 321 (2000).

[8] Jacobs, G., Das, T., Zhang, Y., Li, J., Racoillet, G., Davis, B.H., Fischer-Tropsch Synthesis: Support, Loading, and Promoter Effects on the Reducibility of Cobalt Catalysts, *Applied Catalysis A: General*, **233,** 263 (2002).

[9] Reuel, R.C., Bartholomew, C.H., Effects of Support and Dispersion on the CO Hydrogenation Activity/ Selectivity Properties of Cobalt, *Journal of Catalysis*, **85**, 78 (1984).

[10] Bezemer, G. L., van laak, A., van Dillen, A. J., de Jong, K. P., Cobalt Supported on Carbon Nanofibers- a Promising Novel FT Catalyst, *Journal of Studies In Surface Science and Catalysis*, **147**, 259 (2004).

[11] Serp, P., Corrias, M., Kalck, P., Carbon Nanotubes and Nanofibers in Catalysis, *Applied catalysis A: General*, **253**, 337 (2003).

[12] Tavasoli, A., Sadaghiani, K., Nakhaeipour, A., Ghalbi Ahangari, M., Cobalt Loading Effects on the Structure and Activity for Fischer-Tropsch and Water-Gas Shift Reactions of Co/Al_2O_3 Catalysts, *Iranian Journal of Chemistry and Chemical Engineering*, **26**, 9 (2007).

[13] Tavasoli, A., Mortazavi, Y., Khodadadi, A., Karimi, A., Accelerated Deactivation and Activity Recovery Studies of Ruthenium and Rhenium Promoted Cobalt Catalysts in Fischer-Tropsch Synthesis, *Iranian Journal of Chemistry and Chemical Engineering*, **36**, 25 (2005).

[14] Hilmen, A. M., Schanke, D., Hansesen, K. F., Holmen, A., Study of the Effect of Water on Alumina Supported Cobalt Fischer-Tropsch Catalysts, *Applied Catalysis A: General*, **186**, 169 (1999).

[15] Zhang, J., Chen, J., Li, Y., Sun, Y., Recent Technological Developments in Cobalt Catalysts for FTS, *Journal of Natural Gas Chemistry*, **11**, 99 (2002).